A MOVING MESH ADAPTATION METHOD BY OPTIMAL TRANSPORT

Dongsheng An[1]   Na Lei[2✉]   Tong Zhao[3]   Hang Si[4]   Xianfeng Gu[1]

[1]*Stony Brook University, NY, U.S.A. {doan, gu}@cs.stonybrook.edu*
[2]*Dalian University of Technology, Liaoning, China. nalei@dlut.edu.cn*
[3]*Université Côte d'Azur, Inria, France. tong.zhao@inria.fr*
[4]*Weierstrass Institute for Applied Analysis and Stochastics (WIAS), Berlin, Germany. si@wias-berlin.de*

ABSTRACT

Optimal transportation finds the most economical way to transport one probability measure to another, and it plays an important role in geometric modeling and processing. In this paper, we propose a moving mesh method to generate adaptive meshes by optimal transport. Given an initial mesh and a scalar density function defined on the mesh domain, our method will redistribute the mesh nodes such that they are adapted to the density function. Based on the Brenier theorem, solving an optimal transportation problem is reduced to solving a Monge-Ampère equation, which is difficult to compute due to the high non-linearity. On the other hand, the optimal transportation problem is equivalent to the Alexandrov problem, which can finally induce an effective variational algorithm. Experiments show that our proposed method finds the adaptive mesh quickly and efficiently.

Keywords: Optimal transport, Monge-Ampère equation, Adaptive mesh

1. INTRODUCTION

Motivation The central task in numerical simulation is to solve partial differential equations that model various physical, chemical or biological processes. For dynamic processes, it may be advantageous to vary the resolution dynamically.

Obtaining a numerical approximation to the solution of such problems usually involves generating a mesh. Typically, a uniform-resolution mesh is used. However, if the domain is with complicated geometry, the mesh cannot adequately resolve the small scale features for high curvature regions; or the physical material is highly an-isotropic, the uniform mesh cannot capture the directional feature; or the mesh is evolving, the initial mesh is not conformal to the distorted shape, then the mesh may lead to computational results with poor qualities. In such situations, it is necessary to use dynamic mesh adaptivity to resolve evolving small scale features and other aspects of the solution. Therefore, it is highly desirable to develop a practical computational tool, which can generate adaptive meshes according to monitor functions defined on space-time. One approach is local mesh refinement in which new samples are added to regions where greater resolution is needed. Another approach is mesh relocation, in which the mesh vertices are moved around preserving the connectivity. This work proposes a robust and general-purpose algorithm for generating adaptive meshes based on optimal transportation.

Optimal Transportation Optimal transportation finds the most economical way to transform one probability distribution to another. Recently, optimal transportation has become one of the fundamental tools in geometric modeling and processing. It has been applied for area-preserving parameterizations [1], 3D surface registration and comparison [2], medical image registration [3] and so on. It has been applied broadly

(a) Source measure (Ω, μ) (b) Target measure (Ω^*, ν) (c) Brenier potential u (d) Brenier potential
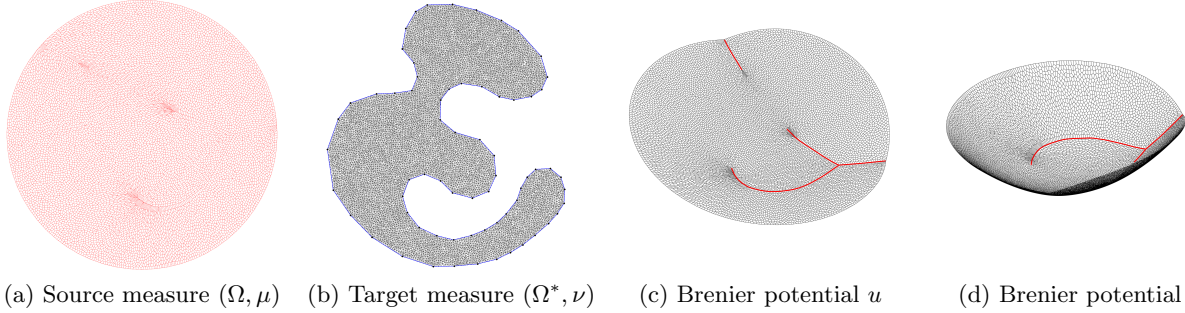
Figure 1: The optimal transportation map $T : (\Omega, \mu) \to (\Omega^*, \nu)$ is the gradient of the Brenier potential $u : \Omega \to \mathbb{R}$.

in generative models in deep learning, e.g. WGAN [4], where the generator computes the optimal transportation map, and the discriminator calculates the Wasserstein distance. It is also used for reflector and refractor design in optics field [5, 6].

For the application of mesh adaption, suppose we are given a geometric domain $\Omega \subset \mathbb{R}^n$, and a desired sampling density function ν defined on Ω. We model ν as the target probability measure, and the uniform distribution μ as the source measure. Then we can compute a unique optimal transportation map $T : \Omega \to \Omega$, such that T maps μ to ν. We uniformly sample the domain Ω and obtain samples $\{p_1, p_2, \ldots, p_n\}$ and map them by the optimal transportation map T. The distribution of the images $\{T(p_1), T(p_2), \ldots, T(p_n)\}$ converges to the prescribed sampling density ν. In this way, we can transform uniform sampling density to any sampling density. The OT method continuously move the locations of the mesh vertices without changing its connectivity. This can effectively avoid the sharp changes in resolution and it has no spurious wave propagation behavior like other methods [7].

Geometric Variational Approach for OT   According to the Brenier's theorem [8], the optimal transportation map is the gradient of a convex function, the so-called Brenier potential. The Brenier potential satisfies the Monge-Ampère equation, which has deep roots in convex geometry and is intrinsically related to the Alexandrov problem [9]. This inspires us to use a geometric variational approach to solve the OT problem. The work in [9] proves that the Brenier theorem is equivalent to the classical Alexandrov theorem in convex geometry. The Alexandrov theorem states that a convex polyhedron is fully determined, uniquely up to a vertical translation, by its face normals and face areas. The Alexandrov polyhedron is in fact equivalent to the graph of the Brenier potential.

In more details, the Alexandrov polyhedron can be constructed as the upper envelope of its supporting planes with known normals and unknown heights. The

projection of the upper envelope induces a power diagram of the plane. We can adjust the heights of the supporting planes to vary the upper envelope, such that the area of each cell in the domain Ω equals to the prescribed area. Alexandrov theorem guarantees the existence and uniqueness (unique up to a vertical translation) of the Alexandrov polyhedron using algebraic topological argument.

The work in [9] gives a variational approach to compute the heights. Geometrically, the vertical lines through the boundary of Ω form a topological cylinder, the xy-plane, the upper envelope and the cylinder together bound a 3-dimensional domain. The volume of this domain minus a linear term gives us a convex energy (Thm. 3.2). The critical point of the energy gives us the Alexandrov polyhedron, namely the Brenier potential. The gradient of the energy equals to the difference between the corresponding target cell areas and the current cell areas, and the each element of the Hessian matrix consists of the length ratio between the corresponding weighted Delaunay triangulation and the power diagram. Therefore, we can use Newton's method to optimize the energy.

Fig. 1 shows an optimal transportation map computed using this method. As shown in frame (a), the source measure μ is the uniform distribution defined on the unit disk Ω; (b) shows the target measure ν, which is also the uniform distribution on a seahorse shaped domain Ω^*. ν is discretized as the summation of Dirac measures, each vertex $y_i \in \Omega^*$ is a sample point with a desired target measure ν_i. Frame (c) and (d) show the convex Brenier potential $u : \Omega \to \mathbb{R}$ from different viewpoints. Its graph is a convex polyhedron (Alexandrov polyhedron), each face is a plane $\pi_i(x) := \langle x, y_i \rangle - h_i$, whose slope is the corresponding sample $y_i \in \Omega^*$, h_i is the unknown height parameter. The projection of Alexandrov polyhedron induces a power diagram of Ω, and the area of the cell corresponding to π_i equals to ν_i.

(a) The given density function   (b) The adaptive mesh   (c) The Brenier potential u (d). The Legendre dual u^*
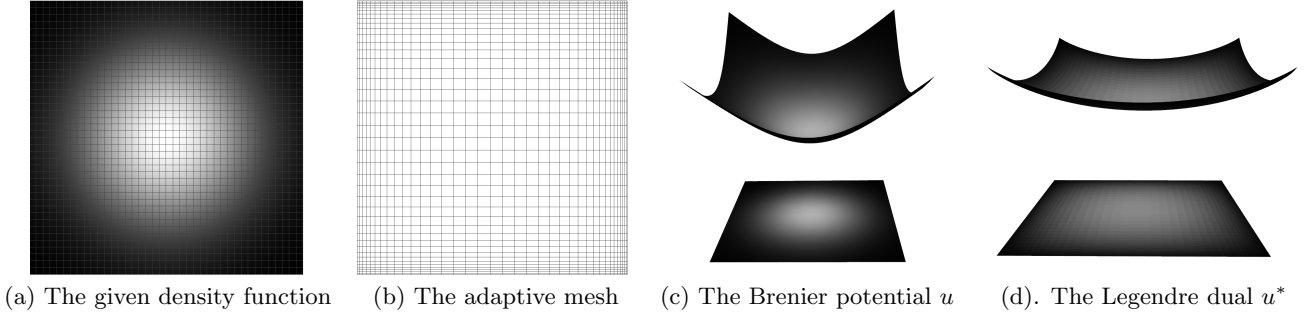
Figure 2: The moving adaptive mesh based on the optimal transportation map. (a) shows the original mesh structure defined on $[0,1]^2$ and the brightness gives the PDF of the function. (b) gives the computed adaptive mesh, in which the cell are is proportional to the brightness of (a). (c) shows the Brenier potential $u : [0,1]^2 \to \mathbb{R}$ and its projection on the source domain. (d) shows the Legendre dual $u^*(y) = \sup_{x \in \mathbb{D}^2} \{\langle x, y \rangle - u(x)\}$.

Contribution The main contribution of the work is to propose to use the optimal transportation method for moving mesh adaption, which maps a uniform distribution to any sampling density, and converts the uniform sampling to the desired sampling. The method has solid theoretic foundation and efficient algorithm based on geometric variational method. The method can be generalized to arbitrary dimension as well.

Notation We define the domain of the fixed computational mesh as Ω, in which the uniform distribution $d\mu = f(x)dx$ is defined. The target domain is given by Ω^* where the positive scalar monitor function $g(y)$ is defined. The monitor function can be treated as a probability density function defined on Ω^* after normalization and is used to represent some physical system of interest, like the climate simulation. We also use x and y to represent positions in Ω and Ω^*, respectively. In the following, we set Ω to be $[-1,1]^2$, and g is discretized on the grids and represented by the discrete measure $\nu = \sum_{i=1}^{n} \nu_i \delta(y - p_i)$, where $\nu_i = 4g(p_i)/\sum_{i=1}^{n} g(p_i)$. Thus, the total measure of μ and ν is equal. Here p_is are the locations of the vertex on Ω^*.

The work is organized in the following way: in section 2, we briefly review the theory, computational algorithms and direct applications of optimal transportation maps; in section 3, we briefly recall Brenier theorem in optimal transportation, Alexandrov theorems in convex geometry, and the geometric variational theorem; in section 4, we explain the details for solving the adaptive mesh generation problem; the experimental results are reported in section 5. Finally the work is concluded in section 6.

2. RELATED WORK

This section briefly reviews the solutions of the adaptive mesh problem and the algorithms of optimal transportation. We refer readers to the textbook [7] for detailed analysis of the moving mesh problem and to [10, 11] for a comprehensive review of the theory and [12] for computational algorithms of the optimal transportation.

2.1 Mesh Generation

There are typically two kinds of methods for the adaptive mesh generation problem, especially when we need the meshes to adequately fit the small scale features. The first class uses a form of local mesh refinement called $h-$adaptivity [13, 14, 15], in which mesh points are adaptively added to the regions where greater resolution is required during the computation. This kind of methods change the connectivity of the vertices in the optimization and thus unstable. The second type method, which is called $r-$adaptivity, continuously move the locations of the mesh vertices without changing its connectivity relationship. By avoiding the sharp changes in resolution, $r-$adaptivity methods has no spurious wave propagation behavior. For detailed reviews, we refer the reader to the textbook [7]. The redistributin of one-dimensional mesh of $r-$adaptivity has been implemented in several software libraries like the bifurcation package AUTO and the currently used weather forecasting software [16, 17]. R-adaptivity has also been applied to the geophysical problems [18, 19, 20]. There is a long history to solve the two-dimensional or three-dimensional $r-$adaptivity problem through optimal transport or the Monge-Ampère equation [21, 22, 23, 24, 25]. Given a prescribed scalar monitor function, these methods find the corresponding adaptive mesh by minimizing a deformation function. In this paper, we adopt the geometric variational method [9] to solve such an equidistribution

problem by computing its corresponding semi-discrete OT map.

2.2 Optimal Transport

Monge raised the optimal transportation map problem as finding the most economical way to transfer one measure to the other in [26]. Kantorovich relaxed the transportation maps to transportation plans and solved the problem using linear programming [27, 28]. Brenier [8] discovered the OT map is the gradient of a convex function, which satisfies the Monge-Ampère equation. Benamou-Brenier [29] developed the theory for computing the OT maps using fluid dynamics. Comprehensive theories on optimal transportation can be found in [11, 30] and so on.

There are many methods for solving the optimal transportation problem, which can be classified into four main categories: Kantorovich approach, Brenier approach, Fluid dynamics approach and discretizing the Monge-Ampère equation approach. The first approach is based on the Kantorovich theorem, the optimal transportation problem is solved by linear programming. De Goes [31] proposed point-to-simplex algorithm similar to linear programming. Sinkhorn [32] method added an entropy regularizer to the Kantorovich potential and greatly improved the efficiency. The heat kernel was used in [32, 33, 34] to approximate the Wasserstein distance. The second approach is based on the Brenier theorem and the Brenier potential can be found by geometric optimization. Aurenhammer et al. [35] connected the OT map with the power diagram in computational geometry. Gu and Yau et al. [36] linked the Brenier theory and the Alexandrov theory, and proposed a geometric variational approach. De Goes et al. found the equivalence between the capacity-constrained Voronoi tessellation and the OT problem in [37]. Levy [38] and Merigot et al. [39] proposed the multi-scale approaches to accelerate the computation based on the Brenier theory for large-scale optimal transportation problems. The third approach is based on fluid dynamic theory. Benamou and Brenier developed a method [40] to solve the Monge-Ampère equation by minimizing the kinetic energy of a flow field. Haker and Tananbaum [3] developed a method to compute the OT maps using fluid dynamics through removing the curl component from the vector field. It is still unclear whether Haker's method can obtain the optimal transportation map for high dimensional cases. The last kind of methods [41, 42] approximated the Monge-Ampère equation and solve the OT problem by discretizing the Hessian matrix. The optimal transportation methods by solving the Monge-Ampère equation have been generalized to spherical cases by [5, 6, 43].

3. THEORETICAL FOUNDATION

In this section, we briefly review the theoretical foundation of optimal transportation, concentrating on the Brenier theorem and the geometric variational method.

3.1 Equidistribution

To solve the moving adaptive mesh problem, we aim to find the map

$$\hat{T}(x) : \Omega \to \Omega^*$$

such that the positive scalar function g is equidistributed, as shown in Fig. 2(a) and Fig. 2(b). If the density function defined on the source domain Ω is given by $d\mu = f(x)dx$, then the equidistribution problem is equivalent to solving the following partial differential equation (PDE):

$$g(y)\ \det J = f(x) \qquad (1)$$

where J is the Jacobian of the map $\hat{T}$ given by:

$$J = \frac{\partial y}{\partial x}$$

The above problem is actually equivalent to finding a measure preserving mapping from $d\mu = f(x)dx$ to $d\nu = g(y)dy$.

Suppose $\Omega, \Omega^* \subset \mathbb{R}^d$ are domains in an Euclidean space, with probability measures μ and ν respectively satisfying the equal total mass condition: $\mu(\Omega) = \nu(\Omega^*)$. The density functions are $d\mu = f(x)dx$ and $d\nu = g(y)dy$. The transportation map $T : \Omega \to \Omega^*$ is *measure preserving*, if for any Borel set $B \subset \Omega^*$,

$$\int_{T^{-1}(B)} d\mu(x) = \int_B d\nu(y),$$

denoted as $T_\#\mu = \nu$. The measure preserving map from μ to ν is not unique. Thus, there are many solutions to the equidistribution problem Eqn. (1). To solve this problem, many constraints or regularizations have been proposed to make the solutions for the $r-$adaptive methods unique. One of the commonly used constraint is to minimize the total transport cost from μ to ν, namely solving the corresponding optimal transportation problem from μ to ν [42].

3.2 Optimal Transportation

Monge raised the *optimal transportation problem*: given the *transportation cost function $c : \Omega \times \Omega^* \to \mathbb{R}^+$*, we aim to find a transportation map $T : \Omega \to \Omega^*$ that minimizes the *total transportation cost*,

$$(MP) \quad \min\left\{ \int_\Omega c(x, T(x))d\mu(x) : T : \Omega \to \Omega^* \ and\ T_\#\mu = \nu \right\}.$$

The above equation gives the Monge problem (MP) and the minimizer is called the *optimal transportation map* (OT map). The transportation cost of the OT map is called the *OT cost* between the measures.

Theorem 3.1 (Brenier Theorem [8]). *Suppose the measures μ and ν are with compact supports $\Omega, \Omega^* \subset \mathbb{R}^d$ respectively, and they have equal total mass $\mu(\Omega) = \nu(\Omega^*)$. Assume the corresponding density functions satisfy $f, g \in L^1(\mathbb{R}^d)$, and the cost function is $c(x, y) = \frac{1}{2}|x - y|^2$, then the optimal transportation map from μ to ν exists and is unique. It is the gradient of a convex function $u : \Omega \to \mathbb{R}$, the so-called Brenier potential, and u is unique up to adding a constant. Then the OT map is given by $T = \nabla u$.*

An example of the Brenier potential is given by Fig. 2(c). If the Brenier potential is C^2, then by measure preserving condition, it satisfies the Monge-Ampère equation,

$$\det D^2 u(x) = \frac{f(x)}{g \circ \nabla u(x)}, \quad s.t. \nabla u(\Omega) = \Omega^*, \quad (2)$$

where $\det D^2 u$ is the determinant of the Hessian matrix of u and the unique OT map is given by $T = \nabla u$.

3.3 Geometric Variational Method

The above Monge-Ampère equation requires the Brenier potential to be at least C^2. If u is not smooth, we can still define the Alexandrov solution of it. The *sub-gradient* of a convex function u at x is defined as

$$\partial u(x) := \left\{ p \in \mathbb{R}^d : u(z) \geq \langle p, z - x \rangle + u(x), \forall z \in \Omega \right\}$$

The sub-gradient defines a set-valued map: $\partial u : \Omega \to \Omega^*$, $x \mapsto \partial u(x)$. We can use the sub-gradient map to replace the gradient map in the Monge-Ampère equation Eqn. (2), and define the Alexandrov Solution as follows:

Definition 3.1 (Alexandrov Solution). If a convex function $u : \Omega \to \mathbb{R}$ satisfies the equation $(\partial u)_{\#}\mu = \nu$, or equivalently $\mu((\partial u)^{-1}(B)) = \nu(B)$, for all Borel set $B \subset \Omega^*$, then u is called an Alexandrov solution to the Monge-Ampère equation Eqn. (2).

The work of [36] gives a geometric variational approach for computing the Alexandrov solution to the semi-discrete optimal transportation problem.

3.4 Semi-discrete Optimal Transportation

Suppose the source measure is (Ω, μ), Ω is a compact convex domain with non-empty interior in $\mathbb{R}^d$, the density function $f(x)$ is continuous. In practice, the target measure (Ω^*, ν) is usually discretized as $\nu =$

$\sum_{i=1}^n \nu_i \delta(y - p_i)$, where $p_1, \ldots, p_n \subset \mathbb{R}^d$ are distinct n points and $\nu_1, \ldots, \nu_n > 0$ so that $\sum_{i=1}^n \nu_i = \mu(\Omega)$. In this situation, the discrete Brenier potential is a piecewise linear convex function. In fact, there exists a *height vector* $\mathbf{h} = (h_1, \ldots, h_n) \in \mathbb{R}^n$, so that the *upper envelope* $u_{\mathbf{h}}$ of the hyper-planes $\pi_i(x) := \langle x, p_i \rangle + h_i$ defined as

$$u_{\mathbf{h}}(x) = \max_{i=1}^n \{\langle x, p_i \rangle + h_i\}, \quad (3)$$

gives the discrete Brenier potential. The projection of the envelope $\text{Env}(\{\pi_i\}_{i=1}^n)$ induces a power diagram,

$$\mathbb{R}^d = \bigcup_{i=1}^n W_i(\mathbf{h}), \quad W_i(\mathbf{h}) := \{x \in \mathbb{R}^d : \nabla u_{\mathbf{h}} = p_i\}.$$

The μ-volume of each cell $\mu(W_i(\mathbf{h}) \cap \Omega) = \nu_i$, and the semi-discrete optimal transportation map is given by $T(x) = \nabla u_{\mathbf{h}}(x)$, or equivalently $T : W_i(\mathbf{h}) \cap \Omega \mapsto p_i \, \forall i = 1, 2, \ldots, n$. The discrete Brenier potential can be obtained by optimizing the following convex energy.

Theorem 3.2 (Gu et al. [36]). *Let Ω be a compact convex domain in $\mathbb{R}^d$, $\{p_1, ..., p_n\}$ be a set of distinct points in $\mathbb{R}^d$ and $f : \Omega \to \mathbb{R}$ be a positive continuous function. Then for any $\nu_1, \ldots, \nu_n > 0$ with $\sum_{i=1}^n \nu_i = \int_\Omega f(x)dx$, there exists $\mathbf{h} = (h_1, h_2, \ldots, h_n) \in \mathbb{R}^n$, unique up to adding a constant $(c, c, \ldots, c)$, so that*

$$\mu(W_i(\mathbf{h}) \cap \Omega) = \int_{W_i(\mathbf{h}) \cap \Omega} f(x)dx = \nu_i \quad \forall i = 1, 2, \ldots, n. \tag{4}$$

The height vector $\mathbf{h}$ is exactly the optimal solver of the following convex function

$$E(\mathbf{h}) = \int_0^{\mathbf{h}} \sum_{i=1}^n \mu(W_i(\mathbf{h}) \cap \Omega)dh_i - \sum_{i=1}^n h_i \nu_i \quad (5)$$

on the open convex set (the admissible solution space)

$$\mathcal{H} = \{\mathbf{h} \in \mathbb{R}^n | \mu(W_i(\mathbf{h}) \cap \Omega) > 0, \ i \in \{1, 2, \ldots, n\}\}$$

$$\cap \left\{ \sum_{i=1}^n h_i = 0 \right\}. \tag{6}$$

Furthermore, the gradient map $\nabla u_{\mathbf{h}}$ minimizes the quadratic cost $\frac{1}{2} \int_\Omega |x - T(x)|^2 f(x)dx$ among all the measure preserving transportation maps $T : (\Omega, \mu) \to (\mathbb{R}^d, \nu = \sum_{i=1}^n \nu_i \delta(y - p_i)), T_{\#}\mu = \nu$.

Finally, we can build the map $\hat{T} : \Omega \to \Omega^*$ as follows: for each cell W_i its corresponding mass cell center is computed as $m_i = \int_{W_i} xd\mu(x)/\nu_i$, then we have the one-to-one map $\hat{T}$ induced by the optimal transport map T from μ to ν: $\hat{T}(m_i) = p_i$, $i = 1, 2, \ldots, n$.

4. COMPUTATIONAL ALGORITHMS

This section explains the algorithmic details to solve the semi-discrete OT problem. The algorithm is implemented using computational geometric method, hence we start with the fundamental concepts in computational geometry [44].

4.1 Basic Concepts from Computational Geometry

A hyperplane in $\mathbb{R}^{d+1}$ is represented as $\pi(x) := \langle p, x \rangle + h$, $x \in \mathbb{R}^d$, $h \in \mathbb{R}$. Given a family of hyperplanes $\{\pi_i(x) = \langle p_i, x \rangle + h_i\}_{i=1}^n$, their *upper envelope* denoted as $\mathrm{Env}(\{\pi_i\}_{i=1}^n)$ is the graph of the function

$$u(x) := \max_{i=1}^n \{\langle p_i, x \rangle + h_i\}.$$

The Legendre dual of u is defined as

$$u^*(y) := \max_{x \in \mathbb{R}^d} \{\langle x, y \rangle - u(x)\}.$$

Each hyperplane $\pi_i(x)$ has a dual point in $\mathbb{R}^{d+1}$, $\pi_i^* := (p_i, -h_i)$, and the graph of u^* is the *lower convex hull* of the dual points $\{\pi_i^*\}_{i=1}^n$, which is also the minimal convex set containing $\{\pi_i^*\}_{i=1}^n$. The projection of the upper envelope induces a *nearest power diagram* $\mathcal{D}(\Omega)$ of Ω given by

$$\Omega = \bigcup_{i=1}^n W_i(u), \ W_i(u) := \{x \in \Omega | \nabla u(x) = p_i\}.$$

The projection of the lower convex hull u^* induces a *nearest weighted Delaunay triangulation* $\mathcal{T}(\Omega^*)$ of Ω^*. $\mathcal{D}(\Omega)$ and $\mathcal{T}(\Omega^*)$ are dual to each other, namely p_i connects p_j in $\mathcal{T}(\Omega^*)$ if and only if $W_i(u)$ is adjacent to $W_j(u)$. Fig. 2(c) and Fig. 2(d) show these basic concepts.

4.2 Algorithm Pipeline

Given the domain Ω^* and the corresponding density function g, we firstly sample from the grids of Ω^*, represented by $\{p_i\}_{i=1}^n$, then the target measure is defined as $\nu = \sum_{i=1}^n \nu_i \delta(y - p_i)$. Here ν_i is computed by $\nu_i = g(p_i), i = 1, 2, \ldots, n$ and then normalized as $\nu_i = \nu_i / \sum_{i=1}^n \nu_i$. Fig. 3(b) gives an example of the target measure, where g is set to be the normal distribution and the intensity of the vertices is given as ν_is. The source measure is set to be the Uniform distribution defined on Ω which is slightly larger than Ω^*, as shown in Fig. 3(a).

The algorithm mainly optimizes the energy $E(\mathbf{h})$ of Eqn. (5) in the admissible solution space $\mathcal{H}$ of Eqn. (6) using Newton's method. At the beginning, the height vector $\mathbf{h}_0$ is initialized as $h_i = \frac{1}{2}(|p_i|^2 - 1)$ for each

---

Algorithm 1: Adaptive mesh generation

Input: The source domain Ω and the corresponding Uniform distribution μ; the density function g and its corresponding rectangular domain Ω^*

Output: The map $\hat{T}$ and the generated adaptive mesh.

Construct the target measure $\nu = \sum_{i=1}^n \nu_i \delta(y - p_i)$ on Ω^* with grid vertices $\{p_i\}_{i=1}^n$, set $\nu_i = g(p_i)$ and then normalize as $\nu_i = \mu(\Omega) \frac{\nu_i}{\sum_{i=1}^n \nu_i}$;

Initialize $h_i = \frac{1}{2}(|p_i|^2 - 1)$;

while *true* **do**

  Compute the lower convex hull of $\{(p_i, -h_i)\}_{i=1}^n$;

  Compute the upper envelope of the planes $\{\langle p_i, x \rangle + h_i\}_{i=1}^n$;

  Project the upper envelope to the plane to get a power diagram $\Omega = \bigcup_{i=1}^n W_i(\mathbf{h})$;

  Compute the μ-volume of each finite cell $w_i(\mathbf{h}) = \mu(W_i(\mathbf{h}))$ using Eqn. (7);

  Compute the gradient of the energy $E(\mathbf{h})$ using Eqn. (8), $\nabla E(\mathbf{h}) = (\nu_i - w_i(\mathbf{h}))$;

  if $\|\nabla E(\mathbf{h})\| < \varepsilon$ **then**

    return h;

  end

  Compute the μ-lengths of the power Voronoi edges $W_i(\mathbf{h}) \cap W_j(\mathbf{h})$;

  Construct the Hessian matrix of the energy $E(\mathbf{h})$:

$$\mathrm{Hess}(E(\mathbf{h}))_{ij} := \frac{\partial^2 E(\mathbf{h})}{\partial h_i \partial h_j} = -\frac{\mu(W_i(\mathbf{h}) \cap W_j(\mathbf{h}))}{|p_i - p_j|}$$

$$\mathrm{Hess}(E(\mathbf{h}))_{ii} := \frac{\partial^2 E(\mathbf{h})}{\partial h_i^2} = \sum_{j \sim i} \frac{\mu(W_i(\mathbf{h}) \cap W_j(\mathbf{h}))}{|p_i - p_j|}$$

  Solve the linear system: $\mathrm{Hess}(E(\mathbf{h}))\mathbf{d} = \nabla E(\mathbf{h})$;

  $\lambda \leftarrow 1$;

  repeat

    if $\mathbf{h} + \lambda \mathbf{d} \notin \mathcal{H}$ **then**

      $\lambda \leftarrow \frac{1}{2}\lambda$;

      continue;

    end

    Compute the power diagram $\mathcal{D}(\mathbf{h} + \lambda \mathbf{d})$;

  until *no empty power cell*;

  Update the height vector $\mathbf{h} \leftarrow \mathbf{h} + \lambda \mathbf{d}$;

end

Compute the cell centers $\{m_i\}_{i=1}^n$ of $\{W_i\}_{i=1}^n$, and we have $\hat{T}(m_i) = p_i$;

Generate the adaptive mesh of $\{m_i\}_{i=1}^n$ according to the connectivity of $\{p_i\}_{i=1}^n$;

vertex p_i. According to the definition of Power dia-

<table>
<tr><td>(a)Source measure</td><td>(b) Target measure</td><td>(c) OT map given by</td><td>(d). The deformed mesh</td></tr>
<tr><td>(Ω, μ)</td><td>$\{(p_i, \nu_i)\}_{i=1}^n$</td><td>$\mathrm{Env}(\pi_i(x))$</td><td>$\hat{T}(m_i) = p_i$</td></tr>
</table>
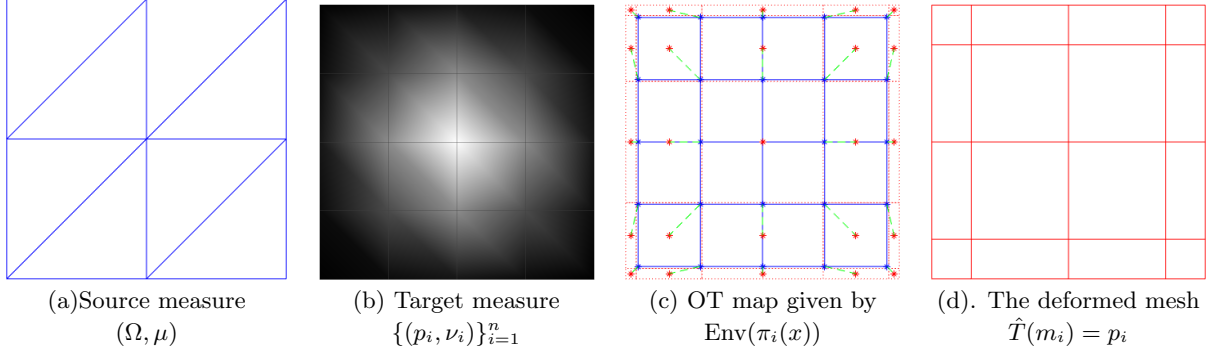
Figure 3: (a) The source domain Ω is with uniform distribution μ. (b) The target measure is defined on the vertices and given by $\nu := \sum_{i=1}^n \nu_i \delta(y - p_i)$. (c) The blue grid gives the original mesh where ν is defined, the dotted red mesh gives the cell decomposition $\{W_i\}_{i=1}^n$ of Ω, with $\mu(W_i) = \nu_i$. The semi-discrete OT map is given by $T : W_i \to p_i$ for all $i = 1, 2, \ldots, n$. Then we map the cell center m_i of W_i (the red stars of Ω) to the corresponding vertex p_i of the target mesh (the blue stars of Ω^*), given by $\hat{T}(m_i) = p_i$. The map relationship is represented by the green dotted lines. (d) We generate the deformed mesh by connecting the cell centers m_i and m_j if the corresponding p_i and p_j are connected in the target measure.

gram, it is easy to show that $\mathbf{h}_0 \in \mathcal{H}$ of Eqn. (6). At each step, the convex hull of $\{(p_i, -h_i)\}_{i=1}^n$ is constructed. The lower convex hull is projected to induce a weighted Delaunay triangulation $\mathcal{T}$ of $\{p_i\}_{i=1}^n$. Each vertex on the convex hull $q_i = (p_i, -h_i)$ corresponds to a supporting plane $\pi_i(\mathbf{h}, x) = \langle p_i, x \rangle + h_i$. Each edge $[q_i, q_j]$ in the convex hull corresponds to the intersection of the hyperplanes π_i and π_j. Each face $[q_i, q_j, q_k]$ in the convex hull is dual to the vertex in the envelope, which is the intersection point of π_i, π_j and π_k. The lower convex hull u^* is dual to the upper envelope u. The projection of the upper envelope u induces the nearest power diagram. The relationship is given in Fig. 2(c) and Fig. 2(d).

To optimize $E(\mathbf{h})$, we compute the μ-volume of each power cell $W_i(\mathbf{h})$ using

$$w_i(\mathbf{h}) := \int_{W_i(\mathbf{h})} f(x)dx, \qquad (7)$$

and the gradient of the energy is given by

$$\nabla E(\mathbf{h}) = (\nu_1 - w_1(\mathbf{h}), \nu_2 - w_2(\mathbf{h}), \ldots, \nu_n - w_n(\mathbf{h})). \qquad (8)$$

The Hessian matrix $\mathrm{Hess}(E(\mathbf{h}))$ for the off diagonal elements of the energy can be constructed as follows:

$$\begin{aligned}\frac{\partial^2 E(\mathbf{h})}{\partial h_i \partial h_j} &= \frac{\partial w_i(\mathbf{h})}{\partial h_j} \\ &= \frac{-1}{|p_i - p_j|} \int_{W_i(\mathbf{h}) \cap W_j(\mathbf{h})} f(x)dx \qquad (9) \\ &= -\frac{\mu(\bar{e}_{ij})}{|e_{ij}|}.\end{aligned}$$

where $f(x)$ is the Uniform distribution defined on Ω, e_{ij} is the edge in the weighted Delaunay triangulation

$\mathcal{T}(\mathbf{h})$ connecting p_i and p_j, $\bar{e}_{ij}$ is the dual edge in the power diagram $\mathcal{D}(\mathbf{h})$, namely the intersection of $W_i(\mathbf{h})$ and $W_j(\mathbf{h})$. The diagonal elements are given as:

$$\frac{\partial^2 E(\mathbf{h})}{\partial h_i^2} = \frac{\partial w_i(\mathbf{h})}{\partial h_i} = \sum_{j \sim i} \frac{\mu(\bar{e}_{ij})}{|e_{ij}|}. \qquad (10)$$

where $\sim$ means the neighbourhood relationship. Then we solve the following linear system to find the update direction,

$$\mathrm{Hess}(E(\mathbf{h}))\mathbf{d} = \nabla E(\mathbf{h}). \qquad (11)$$

Finally, we need to determine the step length λ, such that $\mathbf{h} + \lambda\mathbf{d}$ is still in the admissible solution space $\mathcal{H}$,

$$\mathcal{H} = \{\mathbf{h} \in \mathbb{R}^n | \mu(W_i(\mathbf{h})) > 0, \; i = 1, 2, \ldots, n\}. \qquad (12)$$

We initially set the step length λ to be -1. If $\mathbf{h} + \lambda\mathbf{d}$ is not in the admissible space $\mathcal{H}$, namely some cells disappear in the power diagram $\mathcal{D}(\mathbf{h} + \lambda\mathbf{d})$, then we cut λ to a half, $\lambda \leftarrow 1/2\lambda$, and iterate again. This process is repeated until we find an appropriate step length λ so that $\mathbf{h} + \lambda\mathbf{d}$ is in the admissible space of Eqn. (12). Then we update $\mathbf{h}$ as $\mathbf{h} + \lambda\mathbf{d}$. We repeat the above procedures until the norm of the gradient of the energy is less than a prescribed threshold ε. Each nearest power cell $W_i(\mathbf{h})$ corresponding to the sample point p_i will be of the desired measure ν_i. Then we compute the mass center m_i of each cell W_i and build the map $\hat{T}$ as $\hat{T}(m_i) = p_i$. Finally, the adaptive mesh is constructed as follows: we connect m_i and m_j if p_i and p_j is connected in the target mesh. We conclude our algorithm for solving the moving mesh adaption problem in Alg. 1.

During the optimization, the connectivity of the power diagrams $\mathcal{D}(\mathbf{h})$ keeps changing. Instead of constructing the convex hull u^* from scratch at every step, we

can locally modify the connectivity such as a variation of Lawson's edge flip algorithm [45] can be used to improve the efficiency. Furthermore, in order to improve the numerical stability, we can use adaptive arithmetic during the construction of convex hulls.

Fig. 3(c) gives the computing results of the proposed algorithm with the source measure in Fig. 3(a) and the target discrete measure in Fig. 3(b). The blue mesh of Fig. 3(c) represents the grid structure of $\{p_i\}_{i=1}^n$ and the blue stars are the corresponding vertices of the mesh. The dotted red mesh represents the induced cell decomposition $\{W_i\}_{i=1}^n$ of Ω with $\mu(W_i) = \nu_i$ by the computed OT map from μ to ν. Then we compute the mass center m_i of each cell W_i, given by the red stars. In such a way, we get the one-to-one map that maps p_is to the corresponding m_is, and we show the correspondence relationship by dotted green lines. Finally, we get the deformed mesh through connecting m_i and m_j if (p_i, p_j) is an edge of the given quad mesh, as shown in Fig. 3(d).

5. EXPERIMENTS

We conduct experiments to test the efficacy and efficiency of the proposed OT map algorithm on generating adaptive meshes.

5.1 Experimental setup

All the algorithms are developed using generic C++ compatible with Windows and Linux platforms. We mainly use Eigen [46] for the numerical computations and OpenGL for the user interface. The surface meshes are represented by the half-edge data structure. All the experiments are conducted on a Windows laptop with Intel Core i7-7700HQ CPU and 16 GB memory.

5.2 Source and Target Measures

In order to test the proposed algorithm Alg. 1, we conduct several experiments. The source measure μ is the uniform distribution defined on the planar square $[-1, 1]^2$. We then set four target measures (Ω^*, ν) with $\Omega^* = [-0.9, 0.9]^2$ and $\nu = \sum_{i=1}^n \nu_i \delta(y - p_i)$. Here p_is are defined on the grids of Ω^* and ν_is come from the given density function g, namely $\nu_i = g(p_i)$. For the purpose of visualization, Ω^* is meshed as 41×41 grid. The first model that comes from [42] is the ring model given by

$$g(y) = 1 + 10 sech^2(200\|y\|^2 - 0.25^2)$$

The second is the bell model [42] given by

$$g(y) = 1 + 50 sech^2(100\|y\|^2)$$

The original quad meshes and the corresponding deformed meshes of the ring and the bell models are shown in Fig. 4. It is obvious that the original meshes are deformed according to their given densities. Basically, the grids with higher densities will be enlarged, and those with lower densities will be compressed.

The third asymmetric model comes from the Gaussian mixture model and is given by

$$g(y) = 0.3\mathcal{N}(\mu_1, \Sigma_1^2) + 0.1\mathcal{N}(\mu_2, \Sigma_2^2) + 0.6\mathcal{N}(\mu_3, \Sigma_3^2)$$

where $\mathcal{N}$ represents the Gaussian distribution. $\mu_1 = [-0.5 \ 0.1]^T$, $\Sigma_1 = diag([0.03 \ 0.1])$; $\mu_2 = [0.7 \ 0.3]^T$, $\Sigma_2 = diag([0.1 \ 0.03])$; $\mu_3 = [0.0 \ -0.7]^T$, $\Sigma_3 = diag([0.03 \ 0.03])$. It has three peaks which can be easily recognized from the adaptive mesh (the right frame of the first row of Fig. 5), and the third peak cannot be easily found from the density function image (the left frame of the first row of Fig. 5).

The next model comes from the Franke's function [47], which has two Gaussian peaks of different heights, and a smaller dip:

$$\begin{aligned} g(y) = {} & 0.75 \exp\left(-\frac{(9y_1 - 2)^2}{4} - \frac{(9y_2 - 2)^2}{4}\right) \\ & + 0.75 \exp\left(-\frac{(9y_1 + 1)^2}{49} - \frac{9y_2 + 1}{10}\right) \\ & + 0.5 \exp\left(-\frac{(9y_1 - 7)^2}{4} - \frac{(9y_2 - 3)^2}{4}\right) \\ & - 0.2 \exp\left(-(9y_1 - 4)^2 - (9y_2 - 7)^2\right) \end{aligned}$$

The generated adaptive meshes of the Gaussian mixture function and the Franke's in Fig. 5 also show that the generated meshes fit the density functions well, and the adaptive mesh can be used to identify the small peaks and dips of the given density functions.

Finally, we test on the scalar monitor function given by the grayscale images from Digital Image Processing [48]. The sampling resolution of the target mesh is set to be 400×400. For the purpose of visualization, we simplify the final mesh to be 40×40 (shown in Fig. 6). For the complex density function with high curvatures, our method also works well.

To show the performance of the proposed method in terms of running iterations and running time, we use different resolution of the grids (namely different number of vertices) for the Franke's function. The stopping condition is given as $\max_i(|w_i - \nu_i|/\nu_i) < 1e - 8$ with $w_i = \mu(W_i)$ in Alg. 1. The results are given by Tab. 1. From the table we can find that our method can easily handle the mesh with 401×401 grids with small running iterations.

Furthermore, we show the evolution of the histograms of $\{\log(w_i/\nu_i)\}_{i=1}^n$ in different iterations for

Table 1: The iterations and running time of the proposed method for different number of vertices or different sampling resolution of the Franke's function [47].

Vertex	Iterations	Time (s)
1681	8	0.227
10201	10	1.544
40401	12	7.938
160801	12	53.307

the Franke's function model (401×401 grid) in Fig. 7. If the algorithm converges well, we'll finally get that $w_i = \nu_i$ for all $i = 1, 2, \ldots, n$, namely $\log(w_i/\nu_i) = 0$. Only after seven iterations, the algorithm converges well and nearly all of $\log(w_i/\nu_i)$ concentrates on 0. Also, we give the moving meshes of different iterations in Fig. 8. It is obvious that the mesh moves consistently and does not change a lot even after 5 iterations.

6. CONCLUSION

In this work, we introduce a practical algorithm to solve the adaptive mesh generation problem given the corresponding density function. By dynamically update the locations of the vertices, the proposed method is fast and stable. Our experimental results demonstrate that the proposed method works well for different kinds of density functions and high resolution grids.

References

[1] Zhao X., Su Z., Gu X., Kaufman A. "Area-Preservation Mapping using Optimal Mass Transport." *IEEE Transactions on Visualization and Computer Graphics.*, vol. 19, no. 12, 2838 – 2847, 2013

[2] Su Z., Wang Y., Shi R., Zeng W., Sun J., Luo F., Gu X. "Optimal Mass Transport for Shape Matching and Comparison." *Pattern Analysis and Machine Intelligence, IEEE Transactions on*, vol. 37, no. 11, 2246–2259, 2015

[3] Haker S., Zhu L., Tannenbaum A., Angenent S. "Optimal mass transport for registration and warping." *International Journal of computer vision*, vol. 60, no. 3, 225–240, 2004

[4] Arjovsky M., Chintala S., Bottou L. "Wasserstein generative adversarial networks." *Proceedings of the 34th International Conference on Machine Learning-Volume 70*, pp. 214–223. 2017

[5] Wang X.J. "On the design of a reflector antenna II." *Calculus of Variations and Partial Differential Equations*, vol. 20, no. 3, 329–341, 2004

[6] Wang X.J. "On the design of a reflector antenna." *Inverse problems*, vol. 12, no. 3, 351, 1996

[7] Huang W., Russell R.D. *Adaptive Moving Mesh Methods.* Springer Science+Business Media, LLC, 2011

[8] Brenier Y. "Polar Factorization and Monotone Rearrangement of Vector-Valued Functions." *Communications on Pure and Applied Mathematics*, vol. 44, no. 4, 375–417, 1991

[9] Gu X., Luo F., Sun J., Yau S.T. "Variational principles for Minkowski type problems, discrete optimal transport, and discrete Monge-Ampere equations." *arXiv preprint arXiv:1302.5472*, 2013

[10] Villani C. *Topics in optimal transportation.* 58. American Mathematical Soc., 2003

[11] Villani C. *Optimal transport: old and new*, vol. 338. Springer Science & Business Media, 2008

[12] Peyré G., Cuturi M., et al. "Computational Optimal Transport: With Applications to Data Science." *Foundations and Trends® in Machine Learning*, vol. 11, no. 5-6, 355–607, 2019

[13] Hu Y., Randolphr M. "H-adaptive FE analysis of elasto-plastic non-homogeneous soil with large deformation." *Computers and Geotechnics*, 1998

[14] Rodriguez J., Power H. "h-Adaptive mesh refinement strategy for the boundary element method based on local error analysis." *Engineering Analysis with Boundary Elements*, 2001

[15] Albuquerque D.M.S., Pereira J.M.C., Pereira J.C.F. "Residual Least-Squares Error Estimate for Unstructured h-Adaptive Meshes." *Numerical Heat Transfer, Part B: Fundamentals*, vol. 67, no. 3, 187–210, 2015

[16] Piccolo C., Cullen M. "Adaptive mesh method in the Met Office variational data assimilation system." *Quarterly Journal of the Royal Meteorological Society*, 2011

[17] Piccolo C., Cullen M. "A new implementation of the adaptive mesh transform in the Met Office 3D-Var System." *Quarterly Journal of the Royal Meteorological Society*, 2012

[18] Dietachmayer G.S., Droegemeier K.K. "Application of Continuous Dynamic Grid Adaption Techniques to Meteorological Modeling. Part I: Basic Formulation and Accuracy." *Monthly Weather Review*, 1992

[19] M.Prusaa J., Smolarkiewicz P.K. "An all-scale anelastic model for geophysical flows: dynamic grid deformation." *Journal of Computational Physics*, 2003

[20] Kühnlein C., Smolarkiewicz P.K., Dörnbrack A. "Modelling atmospheric flows with adaptive moving meshes." *Journal of Computational Physics*, 2012

[21] Budd C., Williams J.F. "Moving Mesh Generation Using the Parabolic Monge–Ampère Equation." *SIAM Journal on Scientific Computing*, 2009

[22] Chacón L., Delzanno G.L., Finn J.M. "Robust, multidimensional mesh-motion based on Monge–Kantorovich equidistribution." *Journal of Computational Physics*, 2011

[23] Budd C., Russell R.D., Walsh E. "The Geometry of r-adaptive meshes generated using Optimal Transport Methods." *Journal of Computational Physics*, 2014

[24] Browne P., Budd C., Piccolo C., Cullen M. "Fast three dimensional r-adaptive mesh redistribution." *Journal of Computational Physics*, 2014

[25] Browne P., Prettyman J., Weller H., Pryer T., lent J.V. "Nonlinear solution techniques for solving a Monge-Ampère equation for redistribution of a mesh." *https://arxiv.org/abs/1609.09646*, 2016

[26] Monge G. "Mémoire sur la théorie des déblais et des remblais." *Histoire de l'Académie Royale des Sciences de Paris*, 1781

[27] Kantorovich L. "On a problem of Monge." *Uspekhi Mat. Nauk.*, vol. 3, 225–226, 1948

[28] Kantorovich L.V. "On a problem of Monge." *Journal of Mathematical Sciences*, vol. 133, no. 4, 1383–1383, 2006

[29] Benamou J.D., Brenier Y. "A computational fluid mechanics solution to the Monge-Kantorovich mass transfer problem." *Numerische Mathematik*, vol. 84, no. 3, 375–393, 2000

[30] Santambrogio F. "Optimal transport for applied mathematicians." *Birkäuser, NY*, vol. 55, no. 58-63, 94, 2015

[31] De Goes F., Cohen-Steiner D., Alliez P., Desbrun M. "An optimal transport approach to robust reconstruction and simplification of 2d shapes." *Computer Graphics Forum*, vol. 30, pp. 1593–1602. Wiley Online Library, 2011

[32] Cuturi M. "Sinkhorn distances: Lightspeed computation of optimal transport." *Advances in neural information processing systems*, pp. 2292–2300. 2013

[33] Solomon J., Rustamov R., Guibas L., Butscher A. "Earth mover's distances on discrete surfaces." *ACM Transactions on Graphics (TOG)*, vol. 33, no. 4, 67, 2014

[34] Solomon J., De Goes F., Peyré G., Cuturi M., Butscher A., Nguyen A., Du T., Guibas L. "Convolutional wasserstein distances: Efficient optimal transportation on geometric domains." *ACM Transactions on Graphics (TOG)*, vol. 34, no. 4, 66, 2015

[35] Aurenhammer F. "Power diagrams: properties, algorithms and applications." *SIAM Journal on Computing*, vol. 16, no. 1, 78–96, 1987

[36] Gu X., Luo F., Sun J., Yau S.T. "Variational principles for Minkowski type problems, discrete optimal transport, and discrete Monge–Ampère equations." *Asian Journal of Mathematics*, vol. 20, no. 2, 383–398, 2016

[37] De Goes F., Breeden K., Ostromoukhov V., Desbrun M. "Blue noise through optimal transport." *ACM Transactions on Graphics (TOG)*, vol. 31, no. 6, 171, 2012

[38] Lévy B., Schwindt E.L. "Notions of optimal transport theory and how to implement them on a computer." *Computers & Graphics*, vol. 72, 135–148, 2018

[39] Mérigot Q. "A multiscale approach to optimal transport." *Computer Graphics Forum*, vol. 30, pp. 1583–1592. Wiley Online Library, 2011

[40] Benamou J., Brenier Y., Guittet K. "The Monge-Kantorovitch mass transfer and its computational fluid mechanics formulation." *International Journal for Numerical Methods in Fluids*, 2002

[41] Nader G., Guennebaud G. "Instant Transport Maps on 2D Grids." *ACM Trans. Graph.*, vol. 37, no. 6, 2018

[42] McRae A.T.T., Cotter C.J., Budd C.J. "Optimal-Transport–Based Mesh Adaptivity on the Plane and Sphere Using Finite Elements." *SIAM Journal on Scientific Computing*, 2018

[43] Cui L., Qi X., Wen C., Lei N., Li X., Zhang M., Gu X. "Spherical optimal transportation." *Computer-Aided Design*, vol. 115, 181–193, 2019

[44] Berg M.d., Cheong O., Kreveld M.v., Overmars M. *Computational Geometry: Algorithms and Applications*. Springer-Verlag TELOS, Santa Clara, CA, USA, 3rd ed. edn., 2008

[45] Lawson C.L. "Transforming triangulations." *Discrete Mathematics*, 1972

[46] Guennebaud G., Jacob B., et al. "Eigen v3." http://eigen.tuxfamily.org, 2010

[47] Franke R. "A critical comparison of some methods for interpolation of scattered data." *NAVAL POSTGRADUATE SCHOOL MONTEREY CA*, 1979

[48] Gonzalez R.C., Woods R.E. *Digital Image Processing*. Pearson, 3rd ed. edn., 2007
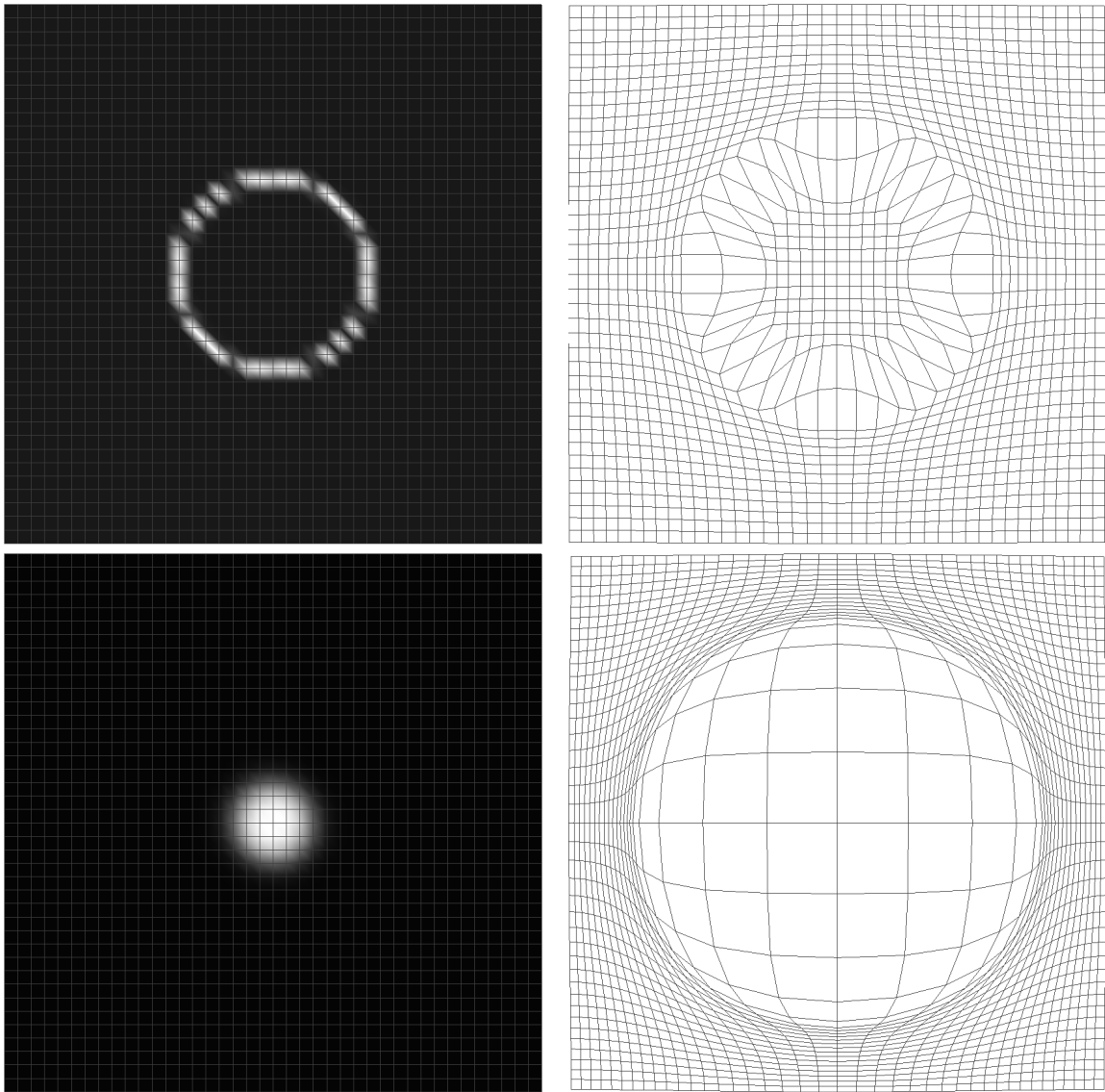
(a) The density functions.   (b) The generated adaptive meshes.

Figure 4: The adaptive meshes of the ring and the bell models [42]. Zoom in/out for better visualization.
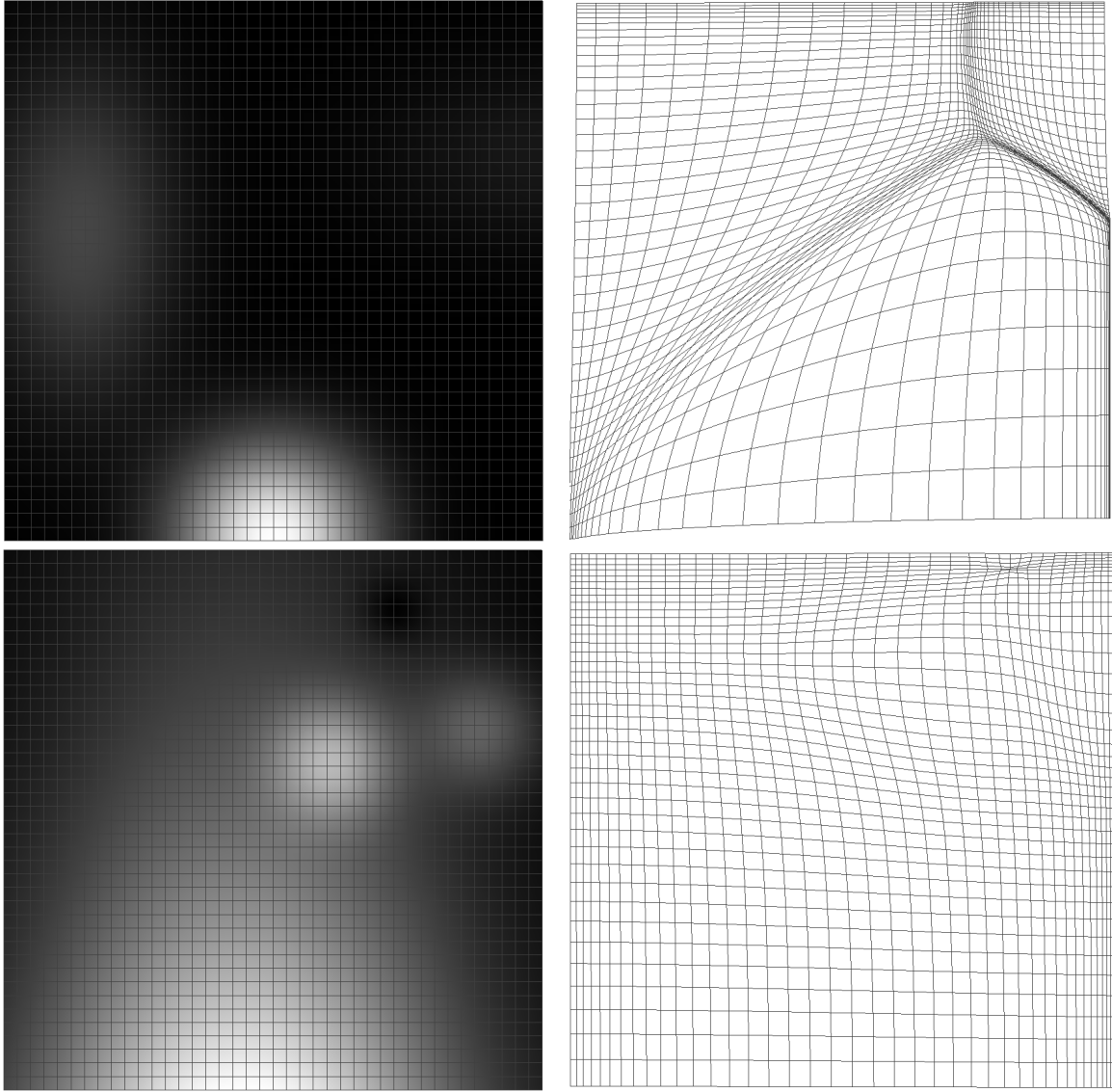
(a) The density functions.   (b) The generated adaptive meshes.

Figure 5: The adaptive meshes of the Gaussian mixture density function and the Franke's function [47]. Zoom in/out for better visualization.
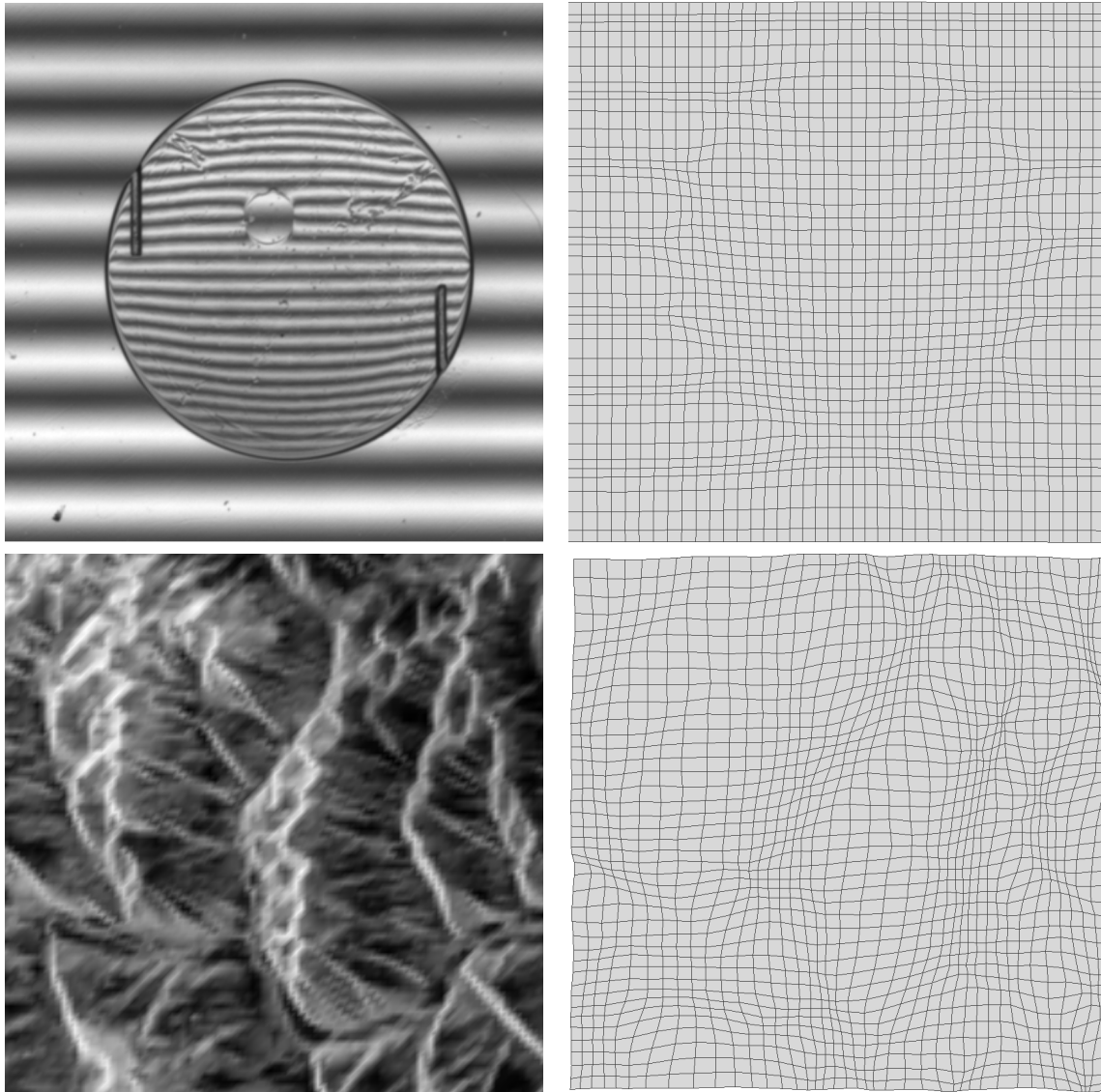
(a) The density functions.   (b) The generated adaptive meshes.

Figure 6: The adaptive meshes of the density function defined by real image in [48]. Zoom in/out for better visualization.
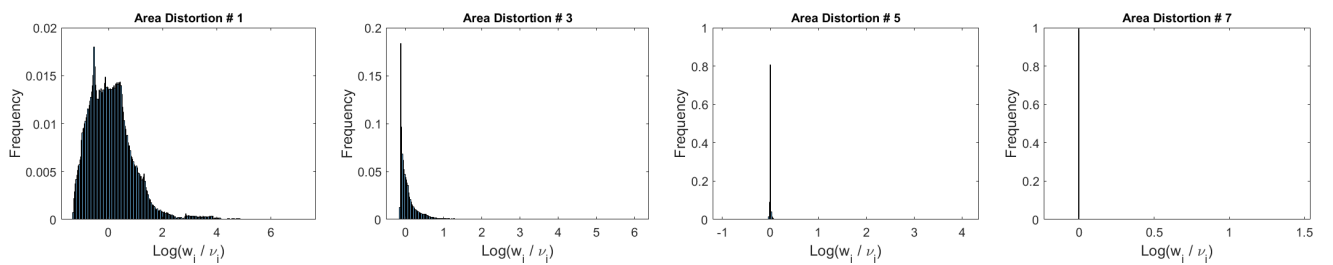

Figure 7: The histograms of the area distortion of the Franke's function model [47] in different iterations of the proposed method. The numbers in the title of each figure shows the corresponding iteration number.
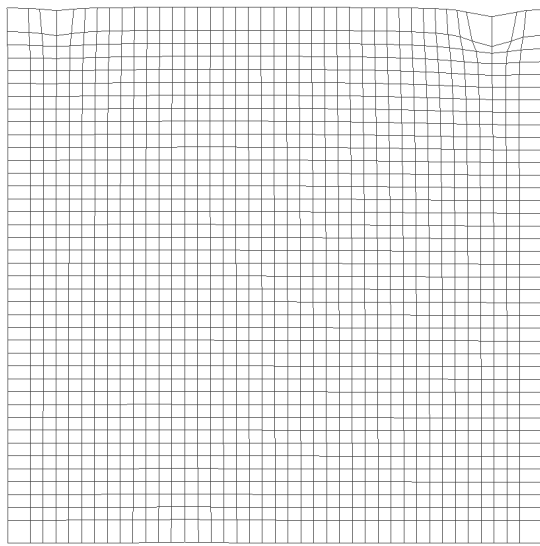
Iter #1
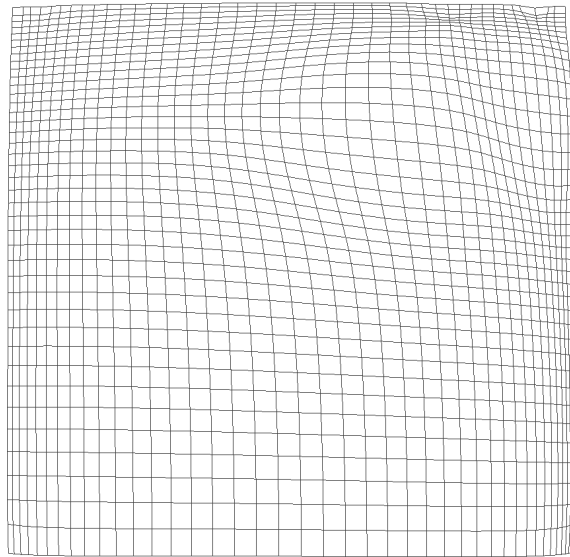
Iter #3
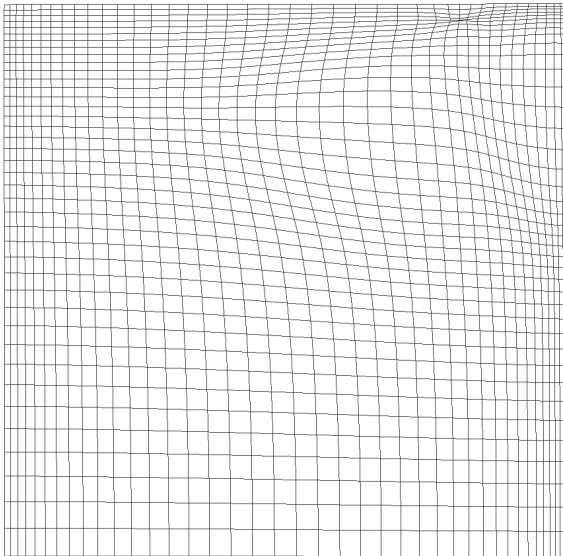
Iter #5
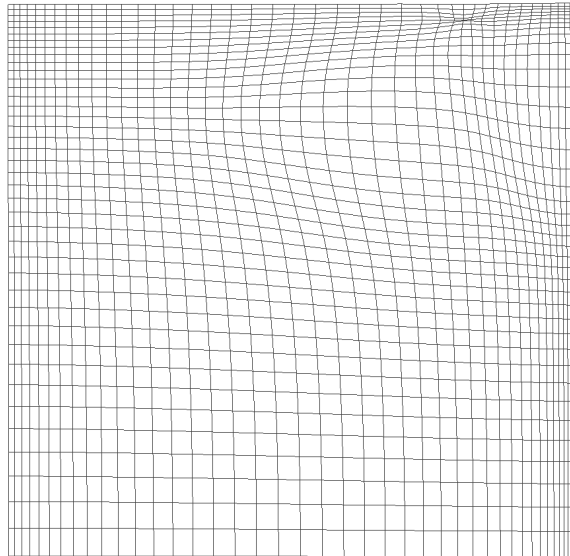
Iter #7

Figure 8: The moving meshes of the Franke's function model [47] in different iterations of the proposed method. The numbers below each figure shows the corresponding iteration number. Zoom in/out for better visualization.